NOVEL BEARINGLESS BRUSHLESS MOTOR IN EXTERIOR ROTOR CONSTRUCTION FOR STIRRED BIOREACTORS

T. Reichert*, T. Nussbaumer †, J.W. Kolar*

**Power Electronic Systems Laboratory, ETH Zurich,8092 Zürich, Switzerland, reichert@lem.ee.ethz.ch*
†Levitronix GmbH, Technoparkstrasse 1, 8005 Zürich, Switzerland

Keywords: Bioreactor stirrer, brushless motor, bearingless motor, exterior rotor, high-torque

Abstract

The paper presents a novel topology for a bearingless permanent magnet motor which is especially qualified for high-torque and yet gentle bioreactor stirring. Both torque and bearing forces are created inside this magnetically levitated disk-shaped motor using a sophisticated control with superimposed coil currents. An optimal design is derived using 3D-FEM analysis and the results are verified with a prototype setup.

1 Introduction

The bearingless slice motor [9,10,12] combines a brushless drive with a magnetic bearing and integrates both components into a single electromagnetic device construction. It has proven its advantageous employment in technology sectors which demand for ultra clean and gentle work procedures that take place inside hermetically sealed enclosures [2,4,8]. Only the rotor is placed inside the process room, whereas the stator and all control and power electronics are placed outside. This completely wear- and lubrication-free concept guaranties long life time and low maintenance costs. In this paper, the concept of the bearingless slice motor is successfully adapted to bioreactor applications.

The stirred vessel is the most commonly used type of bioreactor [1,6,11]. The cell cultures created in the reactor need to be constantly supplied with nutrition and air bubbles. Therefore, one or several high-torque agitators mounted from the bottom have to create a loop flow inside the vessel in order to create a uniform, cell-friendly environment. Alternatively, these agitators could be mounted from the top. However, this would not only limit the available space for inlets and sensor openings at the tank top, it would also require a large head space above the bioreactor in order to assemble and disassemble the impeller units. Therefore, this paper will focus on bottom-mounted agitators.

For state-of-the-art stirred bioreactors, the impeller inside the vessel is connected with an exterior motor by means of a rotating shaft passing through a seal or with a magnetic coupling. However, both seal and magnetic coupling create pinch-off areas that can harm the cell cultures. This impact on the cell destruction can be significantly reduced by employing a bearingless motor which requires no shaft and has no direct contact with the reactor wall (cf. Fig. 1). The impeller blades are mounted onto a disk-shaped rotor consisting of permanent magnets and iron. The stator and all power electronics are placed outside the vessel and both rotation energy and bearing forces are transmitted through the tank wall by means of magnetic forces. Moreover, the large possible air gap makes this motor suitable for clean-in-place (CIP) and sterilization-in-place (SIP) applications [3].

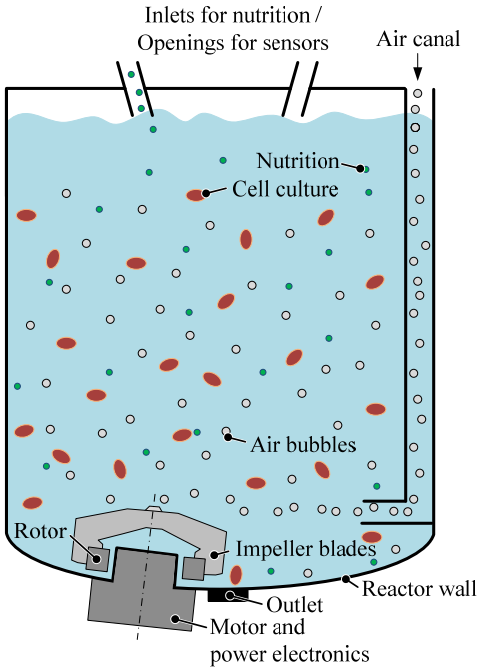

Fig. 1: Schematic view of a stirred bioreactor with a bearingless agitator.

Different feasible motor topologies are discussed and compared in section 2. The best motor topology for the targeted bioreactor applications is then examined in great detail. In section 3, the generation of its torque and bearing forces are explained. A design optimization using 3D-FEM analysis is undertaken in section 4. Finally, the achieved results are verified with a real-size prototype setup.

2 Motor topology

For a targeted bioreactor with a volume range of 500-2000 l, a single bottom-mounted agitator based on the concept of the bearingless slice motor shall be developed. An exterior rotor construction has been chosen, wherefore an indentation in the tank wall is needed (cf. Fig. 1). This construction is advantageous in the case of bottom-mounting, because it

creates no unwanted flow-low zones and it doesn't impact the tank drainage through the main outlet in the middle of the bottom. Moreover, very high torque can be provided with an energy-dense exterior-rotor construction.

Due to the limited available space for the stator parts in the case of an exterior-rotor setup, only a little number of construction possibilities can be considered. A trade-off has to be found between stator iron space and winding space. The torque generation is proportional to the magnetomotive force (measured in ampere-turns At), which is the product of the winding number and the current through it. Obviously, considering a certain maximum allowed current density, with larger space for coils higher magnetomotive force can be provided. However, a minimal stator tooth thickness is required in order to avoid heavy magnetic saturation, which would drastically reduce the torque. Thus, the number of stator slots has to be chosen small in order to leave sufficient space for the windings.

The minimal required stator slot number for a bearingless motor is four. Even though a stable bearing behaviour is feasible with such a topology, it features disadvantageous single-phase drive characteristics with rather large cogging torque.

A topology with five stator slots results in a five-phase drive with low cogging torque. However, there is no magnetical centre point for the bearing. In order to levitate the rotor in its centre position, high bearing currents are needed permanently. Thus, the available power for the drive is limited.

For a slot number of six, a promising topology can been found. In combination with a 16-pole rotor, this motor provides a stable 3-phase bearing that levitates the rotor, while a 3-phase drive control guarantees smooth rotation with almost zero cogging torque.

Motor topologies with stator slot numbers higher than six are not considered any more, since the remaining space for windings would be too small to place coils that can provide sufficient magnetomotive force.

Thus, an exterior-rotor construction with a slot/pole ratio of 6/16 (cf. Fig. 2) has been found to be the optimal choice for the dedicated bioreactor applications. The stator is made of iron and holds one coil on each tooth. The rotor consists of an outer iron ring (back iron) and 16 permanent magnets which are radially magnetized in alternating order.

3 Torque and bearing forces

Together, the drive and magnetic bearing of this novel motor have to control all six degrees of freedom (DOF) of the rotor. The bearing is responsible for five degrees of freedom, leaving the remaining degree of freedom (rotation around its main axis) to the drive control. The bearing forces control the rotor position in radial (2 DOF), axial (1 DOF) and tilting (2 DOF) directions and they can be divided into passive and active forces.

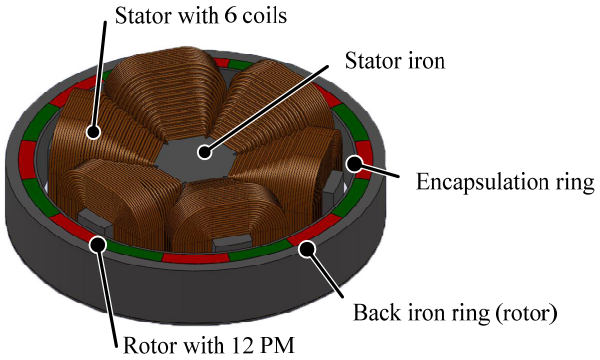

Fig. 2: CAD drawing of the proposed motor topology.

3.1 Passive bearing forces

All five degrees of freedom controlled by the bearing are subject to attracting reluctance forces. In the case of the axial and the tilting positioning, these passive forces are already sufficient to stabilize the rotor [4,8]. Any displacement from the centre position leads to a restoring force. However, this concept is not valid for the two degrees of freedom in radial directions. In the centre position, there is a magnetic equilibrium. But any slight displacement results in a destabilizing force that moves the rotor even further away from its working position until the rotor would finally make contact with the stator (touchdown). Thus, in the case of the radial positioning, an active control has to counteract these destabilizing forces.

The strength of these passive stabilizing and destabilizing forces is mainly determined by the setup, i.e. the combination of permanent magnet and iron material and their dimensions (cf. section 4).

3.2 Active bearing forces

As mentioned before, the radial rotor position can only be controlled by applying active bearing forces, counteracting the destabilizing reluctance forces. There is one stator coil on each stator tooth and with bearing current applied, both radial (referred to as Maxwell forces) and tangential forces (referred to as Lorentz forces) can be generated. All these forces are then superimposed and the resulting force shows into the desired direction, counteracting the destabilizing passive force.

In practice, the active bearing is distributed into its two degrees of freedom in order to control radial displacement in x-direction and y-direction separately. The control for both cases can be done individually and the resulting bearing currents will be superimposed in the end prior to applying them to the stator coils.

The resulting bearing currents for both x- and y- direction are highly dependent on the actual rotation angle

$$\alpha_{elec} = p \cdot \alpha_{mech}, \tag{1}$$

which is the product of pole pair number p and the mechanical rotation angle α_{mech}.

For this bearing, three non-adjacent stator teeth together build a three-phase system (e.g.. coil 1, 3 and 5) in terms of the applied current, whereas for two opposite coils the currents are always phase-shifted by 180 degrees (cf. Fig. 3). The amplitude of these bearing currents is determined by a PID controller depending on the radial displacement. Thus, both the rotation angle and the radial displacement have to be measured constantly.

Fig. 3 shows the generation of a force into the positive x-direction for two specific rotation angles. The partial force of each coil can be stated as

$$F_{n,x}(\alpha_{elec}) = k_{Fn,x} \cdot \cos(\alpha_{elec} + (n-1)\cdot 60°) \cdot N_{coil} \cdot \hat{I}_{bng}\,, \quad (2)$$

with the bearing-current factor per coil $k_{Fn,x}$ in x-direction, the winding number N_{coil} and the amplitude of the bearing current $\hat{I}_{bng}$. The total resulting force is then given by

$$F_x = \sum_{n=1}^{6} F_{n,x}\,. \quad (3)$$

The same force calculation can be done in y-direction, where the partial force of each coil becomes

$$F_{n,y}(\alpha_{elec}) = k_{Fn,y} \cdot \sin(\alpha_{elec} + (n-1)\cdot 60°) \cdot N_{coil} \cdot \hat{I}_{bng}\,, \quad (4)$$

with the bearing-current factor per coil $k_{Fn,y}$ in y-direction.

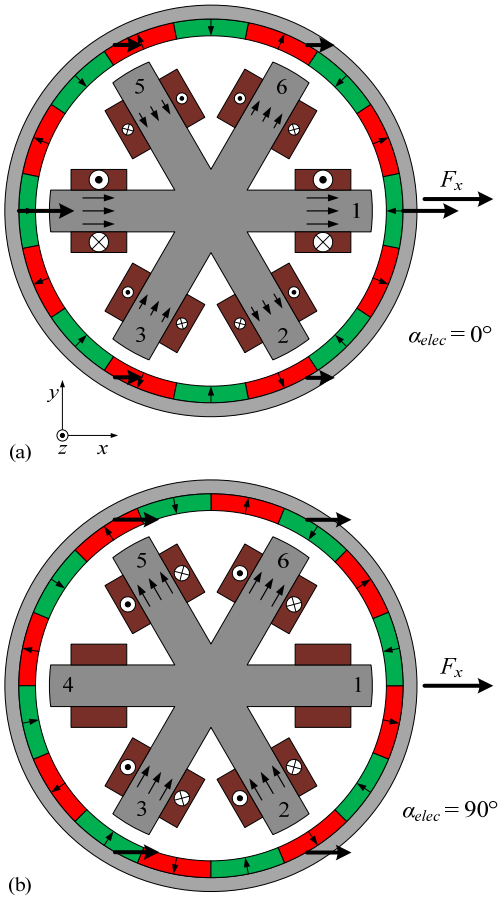

Fig. 3: Radial force generation in x-direction for two specific rotation angles: (a) $\alpha_{elec} = 0°$; (b) $\alpha_{elec} = 90°$.

3.3 Drive control and torque generation

The remaining degree of freedom is the rotation around the main axis of the rotor. For the control, another three-phase system has to be implemented. However, only tangential forces are desired, since radial forces cannot contribute to any torque generation and would only disturb the bearing. Similar to the bearing control, three non-adjacent coils build one three phase system. This time however, the currents in two opposite coils have no phase-shift and both coils contribute to the torque equally. With the employed three-phase drive smooth rotation is guaranteed.

In Fig. 4, the torque generation is explained using the example of the same two specific rotation angles. Each coil contributes to the torque with

$$T_n(\alpha_{elec}) = k_T \cdot \sin^2(\alpha_{elec} + (n-1)\cdot 120°) \cdot N_{coil} \cdot \hat{I}_{drv}\,, \quad (5)$$

with the torque-current factor k_T (equal for all coils) the amplitude of the drive current $\hat{I}_{drv}$. The total torque becomes

$$T = \sum_{n=1}^{6} T_n = \underbrace{\kappa_T}_{3\cdot k_T} \cdot N_{coil} \cdot \hat{I}_{drv}\,, \quad (6)$$

with an overall torque-current constant κ_T and the winding number N_{coil}, which is the same for both drive and bearing since we will only have one coil on each stator tooth.

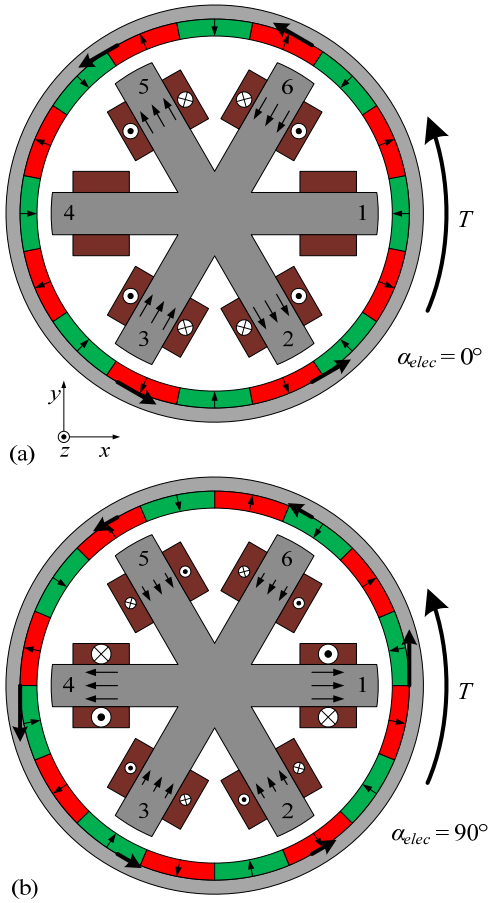

Fig. 4: Torque generation for two specific rotation angles: (a) $\alpha_{elec} = 0°$; (b) $\alpha_{elec} = 90°$.

3.4 Superposition for rotor control

Up to now, the active bearing and the drive control have been looked at separately, whereas for operation both control systems need to work simultaneously. This could be achieved by putting two coils onto each stator teeth, one for the bearing and one for the drive and run the two control systems on separate coils. However, if in certain rotor constellations drive and bearing want to produce forces contrary to each other, high currents are applied and yet a large part of the forces cancel each other out. Therefore, it is recommended to use only one coil per stator teeth and to mathematically superimpose the required control currents already in the control unit [7].

4 Design optimization

The proposed 6-slot/16-pole topology has been optimized using 3D-FEM analysis. All geometric variables (listed in Table 1) have been considered in order to find a motor design that can provide both high torque (up to 20 Nm are needed for the targeted reactor volume) and sufficient bearing forces.

The limiting space factor for the whole stirrer is the outer diameter of the impeller, which is set to 170 mm for the targeted reactor size. With a minimal blade length of 10 mm per side, the outer diameter of the rotor is limited to 150 mm. This available space has to be optimally divided into rotor and stator parts and into the air gap length, whereby a minimal radial magnetical air gap length of 5 mm (resulting in an actual mechanical air gap length of 1-2 mm after considering the required space for the tank wall and both rotor and stator encapsulation) is necessary in order to comply with the CIP and SIP requirements.

4.1 Shape of the stator teeth

Usually, a stator consists of several stator teeth, each opening up towards the rotor into a tooth tip [cf. Fig. 5(a)]. Thus, three variables have to be determined for the stator design, i.e. the stator tooth width w_t, the tooth tip opening angle α_{tt} and the radial tooth tip depth δ_{tt}. The evaluation of an optimal design revealed that high torque can be achieved for tooth tip opening angles that lead to a tooth tip arc length which correspond with the stator tooth width

$$r_S \cdot \alpha_t \approx w_t \,, \tag{7}$$

for any stator radius r_S. This means, that an optimal tooth tip thickness is very similar to the actual tooth thickness itself. The optimization can thus be simplified by neglecting the tooth tip and simply considering bar-shaped stator teeth with a single variable, the tooth width w_t [(cf. Fig. 5(b)].

This interesting relation can be associated with magnetic saturation in the iron. If a machine is optimized for high-torque performance, it will always have a working point where the iron material is at the edge of saturation. The tooth tip opening angle for a rotor with 16 permanent magnets has to be rather small, because the tooth tip should cover about one entire magnet in order to gather a high magnetic flux density [5]. If the tooth tip was enlarged, it would cover more than one magnet and the magnetic flux would short-circuit over the tooth tip, reducing the interaction with the flux created by the coils around the stator teeth. The tooth itself on the other hand requires a certain thickness since it has to carry the magnetic flux of the permanent magnets and the flux created by the coil around it. Thus, an optimum can be found when the thickness of the stator tooth and the arc length of the tooth tip approach, leading to the aforementioned result of bar-shaped stator teeth.

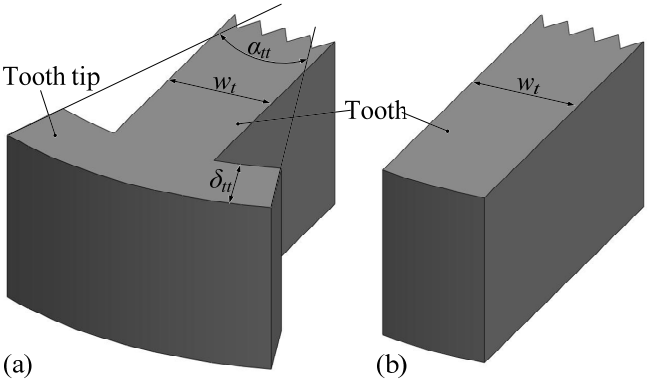

Fig. 5: Shape of a stator teeth for a regular motor (a) and for the proposed bearingless motor (b).

In Fig. 6(a), the resulting torque is analyzed using 3D-FEM analysis for the case when both stator tooth width and magnetomotive force are varied for fixed rotor dimensions. It can be seen that the variation in stator tooth width has a large influence for high magnetomotive force (5000 At). With an optimal stator tooth with of 15 mm, the targeted torque of 20 Nm can be achieved, whereas for other stator dimensions the resulting torque is limited due to magnetic saturation.

In terms of the passive bearing forces, this reduction of iron material facing the rotor is rather critical because it lowers the reluctance forces as can be seen in Fig. 6(b). Even though this is advantageous for the radial bearing, it weakens the axial and the tilting stiffness and thus endangers the overall bearing stability. Minimal values for both axial and tilting stiffness have to be guaranteed. With the chosen stator tooth width of 15 mm, the passive stiffnesses are rather weak but still sufficient for operation.

4.2 Optimal rotor design parameters

Besides the tooth width w_t, mainly radial measurements determine the final design of the motor. The air gap was already set to 5 mm. Thus, the remaining radial space is 148 mm when we consider a 1 mm steel encapsulation around the rotor. It has to be split into rotor (with inner radius r_{Ri}) and stator (with radius r_S) space. However, it is sufficient to focus on the inner rotor radius since this will automatically determine the stator radius as well. The rotor itself will then be divided into magnet material (with thickness δ_{PM}) and iron material (with thickness δ_{BI}). A trade-off has to be found between energy-dense magnet material and sufficient space for back iron in order to avoid heavy saturation. Moreover, the stator needs to be rather large in order to carry the six

stator coils, which need to withstand high currents. Another key parameter is thus the current i_{coil} energizing the stator coils. The product of this current with the winding number N_{coil} is the magnetomotive force Θ that drives the magnetic flux through the stator iron.

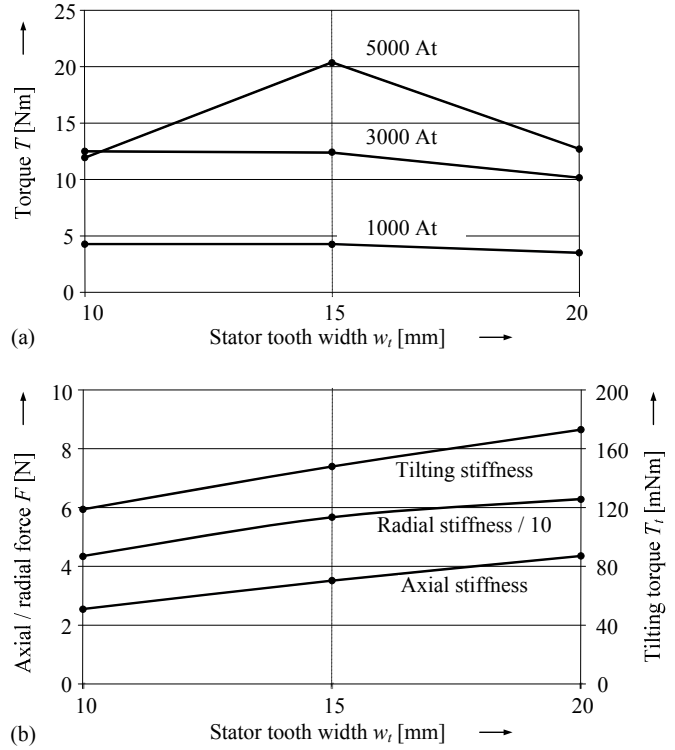

Fig. 6: Comparison of torque (a) and passive stiffnesses (b) for varying stator tooth width. In (a), the difference in torque becomes mainly visible for high magnetomotive force (5000 At), where magnetic saturation is dominant for both small and large tooth width. For a value of 15 mm, the targeted torque of 20 Nm can be reached. In (b), it can be seen that all stiffnesses are lowered with smaller tooth width which is advantageous for the radial bearing but disadvantageous for tilting and axial stiffness.

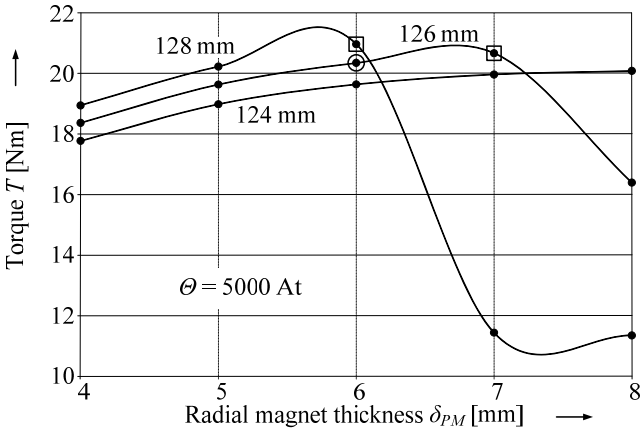

Fig. 7: Optimisation of torque generation for different rotor dimensions [varying magnet thickness and different inner rotor diameters (124-128 mm)]. The stator tooth width is set to 15 mm and the amplitude of the magnetomotive force applied to each coil is 5000 At.

An exemplary optimization result for different rotor measurements simulated with 3D-FEM analysis is shown in Fig. 7. Both the radial magnet thickness and the inner rotor diameter are varied and the resulting torque is plotted in the case of an excitation with amplitude of 5000 At. The two results marked with a box are at the limit of heavy magnetic saturation. Thus, the design point marked with a circle has been chosen in order to guarantee a minimal saturation reserve.

The new motor has been analyzed with 3D-FEM using the newly found optimal parameters, which are summarized in Table 1. Fig. 8 shows the resulting torque and radial bearing forces for the proposed optimal design. It can be seen in Fig. 8(a) that the torque raises until the magnetomotive force exceeds 5500 At. From that point on, magnetic saturation will impact the outcome of the torque generation. In Fig. 8(b), the radial bearing is analyzed. With no external force applied (0 At), the radial force is zero in the centre position but grows negatively when the rotor is displaced. Thus, magnetomotive force has to be applied until the total radial force acting on the rotor becomes positive again and brings the rotor back to its origin position in the centre.

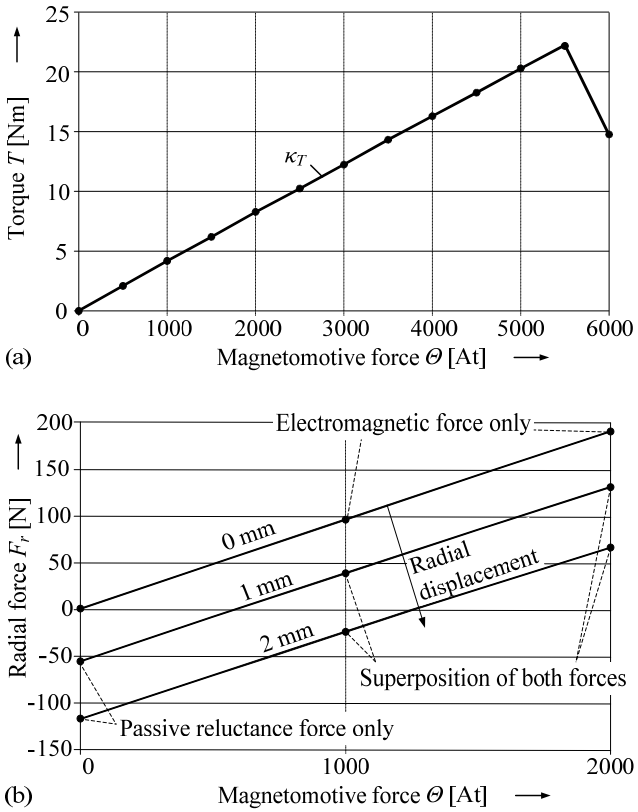

Fig. 8: Analysis of torque (a) and radial bearing forces (b) for the proposed motor dimensions. In (a), the torque grows with the magnetomotive force (with constant κ_T) until magnetic saturation becomes too large (at 6000 At). In (b), the radial force is plotted for different radial rotor displacements (0-2 mm). With no current applied, it can be seen that no radial force is created in the centre position. However, a negative passive reluctance force grows proportionally with the radial displacement. Thus, a magnetomotive force has to be applied accordingly to all coils in order to create a positive force that brings the rotor back to its origin position.

Parameter	Symbol	Value
Stator slot number	q	6
Pole number	$2p$	16
Outer rotor diameter	d_R	148 mm
Air gap thickness	δ_a	5 mm
Inner rotor diameter	d_{Ri}	126 mm
Magnet thickness	δ_{PM}	6 mm
Back iron thickness	δ_{BI}	5 mm
Stator tooth width	w_t	15 mm
Rated torque	T	20 Nm
Rated speed	n	500 rpm

Table 1: Optimal design parameters of the novel bearingless stirrer motor.

5 Verification with prototype setup

A real-size prototype has been built in order to verify the proper functioning of the motor and to evaluate its performance. In Fig. 10, the bearingless motor is shown during levitation. The combined, concentrated coils have to be wound in a cuneiform shape so that the largest possible copper volume can be filled into the available stator space.

The results of a practical test are presented in Fig. 9, showing the measurements of the current in one coil and the radial position signals. In the beginning, the rotor is levitated during standstill (0 rpm). It can be seen, that the radial position is very stable and yet low current is needed in order to stabilise the rotor. Next, the rotor is accelerated to 500 rpm. During this short phase, a high drive current can be measured, which is lower again once the final rotation speed is reached. Since no external torque is applied during rotation with 500 rpm, the current measured in the coil is mainly due to the bearing, which is harder to control now because of destabilizing centrifugal forces. The measurements reveal that the rotor is never displaced more than 60 µm from its centre position which is considerably stable. In the end, the rotor is actively decelerated (again with high drive current) back to 0 rpm.

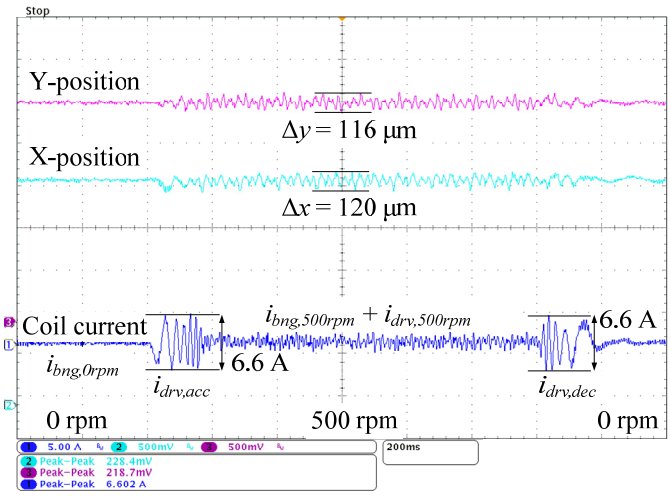

Fig. 9: Measurements of the current in one coil and of the two position signals during a test operation with rotation speeds from 0 to 500 rpm and back to standstill. (Current-scale: 5 A/div., position-scales: 500 mV/div. ≈ 265µm/div., time-scale: 200ms/div.)

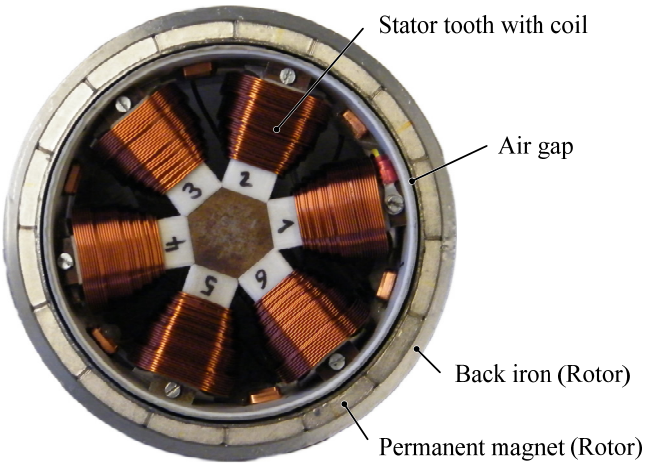

Fig. 10: Real-size prototype of the novel stirrer motor.

Conclusions

A high-torque exterior-rotor bearingless motor has been developed, analyzed, optimized and successfully tested in a real-size setup. It consists of combined winding that generate both torque and bearing forces, leading to an optimized power balance. This novel motor is especially dedicated for stirring in bioreactors where it helps reducing the impact on cell destruction.

References

[1] J. A. Asenjo and J. C. Merchuk, *Bioreactor System Design*, Marcel Dekker, Inc, New York, 1995.

[2] J. Boehm, R. Gerber, J. R. Hartley and S. Whitley, "Development of active magnetic bearings for high speed rotors," *IEEE Trans. Magn.*, vol. 26, pp. 2544-2546, 1990.

[3] Y. Christi and M. Moo-Young, "Clean-in-place systems for industrial bioreactors: Design, validation and operation," *Journal of Industrial Microbiology and Biotechnology,* vol. 13, pp. 201-207, 1994.

[4] P. Karutz, T. Nussbaumer, W. Gruber, J. W. Kolar, „Novel Magnetically Levitated Two-Level Motor," *IEEE/ASME Trans. Mechatronics,* vol. 13, pp. 658-668, 2008.

[5] P. Karutz, T. Nussbaumer, W. Gruber, J. W. Kolar, "Saturation Effects in High Acceleration Bearingless Slice Motors, " Proc. of the 2008 *IEEE International Symposium on Industrial Electronics*, pp. 472-477, 2008.

[6] S. S. Ozturk and W.-S. Hu, *Cell culture technology for pharmaceutical* and cell-based therapies, Taylor & Francis, Boca Raton, 2006.

[7] K. Raggl, T. Nussbaumer, J. W. Kolar "Comparison of Separated and Combined Winding Concepts for Bearingless Centrifugal Pumps", *Journal of Power Electronics*, vol. 9, no. 2, pp. 243-258, 2009.

[8] T. Schneeberger, T. Nussbaumer and J. W. Kolar, "Magnetically Levitated Homopolar Hollow-Shaft Motor," *IEEE/ASME Trans. Mechatronics,* vol. 15, pp. 97-107, 2010.

[9] R. Schoeb and N. Barletta, "Principle and Application of a Bearingless Slice Motor," *JSME international journal. Series C, Mechanical systems, machine elements and manufacturing,* vol. 40, pp. 593-598, 1997.

[10] S. Silber, W. Amrhein, P. Bösch, R. Schoeb, N. Barletta. "Design aspects of bearingless slice motors," *IEEE/ASME Trans. Mechatronics*, vol. 10, no. 6, pp. 611-617, Dec. 2005.

[11] K. van't Riet and J. Tramper, *Basic Bioreactor Design*, Marcel Dekker, Inc, New York, 1991.

[12] N. Watanabe, H. Sugimoto, A. Chiba, T. Fukao and M. Takemoto, "Basic characteristic of a multi-consequent-pole bearingless motor," in *Proc. Power Convers. Conf.-Nagoya, PCC'07,* pp. 1565-1570, 2007.